Remote Sensing of Environment 115 (2011) 3355–3366

Contents lists available at ScienceDirect

Remote Sensing of Environment

journal homepage: www.elsevier.com/locate/rse

Fractional snow cover mapping through artificial neural network analysis of MODIS surface reflectance

Iliyana D. Dobreva *, Andrew G. Klein

[a] Department of Geography, MS 3147, Texas A&M University, College Station, TX 77843-3147, USA

ARTICLE INFO

Article history:
Received 30 March 2011
Received in revised form 25 July 2011
Accepted 30 July 2011
Available online 13 September 2011

Keywords:
Snow fraction
Snow cover
Artificial neural networks
MODIS

ABSTRACT

Accurate areal measurements of snow cover extent are important for hydrological and climate modeling. The traditional method of mapping snow cover is binary where a pixel is considered either snow-covered or snow-free. Fractional snow cover (FSC) mapping can achieve a more precise estimate of areal snow cover extent by estimating the fraction of a pixel that is snow-covered. The most common snow fraction methods applied to Moderate Resolution Imaging Spectroradiometer (MODIS) images have been spectral unmixing and an empirical Normalized Difference Snow Index (NDSI). Machine learning is an alternative for estimating FSC as artificial neural networks (ANNs) have been successfully used for estimating the subpixel abundances of other surfaces. The advantages of ANNs are that they can easily incorporate auxiliary information such as land cover type and are capable of learning nonlinear relationships between surface reflectance and snow fraction. ANNs are especially applicable to mapping snow cover extent in forested areas where spatial mixing of surface components is nonlinear. This study developed a multilayer feed-forward ANN trained through backpropagation to estimate FSC using MODIS surface reflectance, NDSI, Normalized Difference Vegetation Index (NDVI) and land cover as inputs. The ANN was trained and validated with higher spatial-resolution FSC maps derived from Landsat Enhanced Thematic Mapper Plus (ETM+) binary snow cover maps. Testing of the network was accomplished over training and independent test areas. The developed network performed adequately with RMSE of 12% over training areas and slightly less accurately over the independent test scenes with RMSE of 14%. The developed ANN also compared favorably to the standard MODIS FSC product. The study also presents a comprehensive validation of the standard MODIS snow fraction product whose performance was found to be similar to that of the ANN.

1. Introduction

Snow cover has important implications for the hydrology and climate of mid- to high-latitude and mountain environments. As a frozen-water reservoir, snow holds precipitation until snowmelt runoff is released. Snowmelt runoff can pose a flooding hazard because it is often released rapidly during spring (Rango, 1996). However, snow is essential for the water supply of more than one-sixth of world's population that relies on fresh water from seasonal and glacial snowmelt (Barnett et al., 2005), including over 60 million people in the western United States (Bales et al., 2006). Runoff predictions from snowmelt are made by including snow cover information in hydrological models.

Runoff from snow also supplies the necessary water for sustaining forest ecosystems in watersheds (Douville et al., 2002). There is a recognized need to incorporate snow cover extent and Snow Water Equivalent (SWE) within hydrologic models to derive snowmelt runoff estimates for improved forecast accuracy for water supply, runoff rates and soil moisture recharge (Dozier, 1992). Thus, various snowmelt algorithms incorporate information about the evolution of snow covered areas during the winter season (Liston, 1999).

Snow is also an important component of the climate system because of its characteristically high albedo in the visible and near-infrared portions of the electromagnetic spectrum. It reflects most of the incoming solar radiation which in turn modifies the energy exchanges between the Earth's surface and the atmosphere over snow covered areas causing these areas to experience lower temperatures than those without a snowpack (Arnfield, 2006). Snow is also a poor conductor of heat, and snow cover acts as an insulator not allowing the release of heat from Earth (Berry, 1981).

Because snow cover affects energy exchanges at the surface, the areal extent of snow cover is incorporated in General Circulation Models (GCMs) and in weather forecasting models (Marshall et al., 1994; Roesch et al., 2001). However, difficulties arise in modeling the snow's interactions with the atmosphere when inaccurate estimates of snow cover extent are incorporated into climate models (Niu & Yang, 2007). For example, a warm bias over snow covered regions in

* Corresponding author. Tel.: +9794580864.
E-mail addresses: iliyanad@tamu.edu (I.D. Dobreva), klein@geog.tamu.edu (A.G. Klein).

0034-4257/$ – see front matter © 2011 Elsevier Inc. All rights reserved.
doi:10.1016/j.rse.2011.07.018

several of the National Center for Atmospheric Research Community Land Models has been attributed to inaccurate estimates of snow cover extent inputs (Dickinson et al., 2006).

Remote sensing is the most appropriate tool for monitoring snow cover extent because of the large spatial extent and remoteness of snow covered areas, and the adverse weather conditions typical of winters (Derksen & LeDrew, 2000). A further advantage of satellite remote sensing for snow cover mapping is that it offers consistent data collection over large areas. In this respect, long term studies and environmental models have a continuous supply of snow cover measurements (König et al., 2001).

Traditional snow cover maps are binary where each pixel is mapped as either snow-covered or snow-free. The current standard algorithm for producing global daily snow cover maps from Moderate Resolution Imaging Spectroradiometer (MODIS) uses Normalized Difference Snow Index (NDSI) as a threshold to delineate snow. A Normalized Difference Vegetation Index (NDVI) threshold is also used to improve snow detection in forests (Hall et al., 1995, 2002; Klein et al., 1998).

Fractional snow cover (FSC) maps provide an enhancement to the binary maps. A pixel contains the spectral information from all surface components within a sensor's Instantaneous Field Of View (IFOV) and a number of approaches have been developed to estimate the percentage of the snow component in a pixel. Even so, the snowpack cannot be spatially located within a pixel because spectral information is integrated over the entire IFOV. Estimating the snow covered fraction of pixels represents an improvement over binary snow cover maps where a pixel is ideally classified as containing snow if at least approximately fifty percent of its area is snow-covered (Hall et al., 2002).

The most common approach to estimating FSC is linear mixture analysis which is performed under the assumption that the reflectance of a pixel is a linear combination of the surface components within that pixel and that the weight of each component is proportional to the percent of the pixel's IFOV containing that component (Jensen, 2005). These endmembers are idealized, pure spectral signatures for a surface type (Schowengerdt, 1997). The performance of the spectral unmixing model depends on availability of complete and accurate endmembers. The method has been applied extensively in snow fraction mapping (Foppa et al., 2004; Hongen & Suhong, 2004; Metsamaki et al., 2005; Nolin & Dozier, 1993; Painter et al., 2003, 2009; Romanov et al., 2003; Shi, 1999; Simpson et al., 1998; Simpson & McIntire, 2001; Vikhamar & Solberg, 2002, 2003). These studies differ on how endmembers are collected and how the mapping algorithm determines which endmembers should be included in unmixing each pixel to determine FSC.

Another approach to snow fraction mapping has been through development of an empirical relationship between satellite reflectance and FSC. A method developed for images from the Terra and Aqua MODIS instruments (Salomonson & Appel, 2004, 2006) uses the NDSI constructed from MODIS bands 4 (0.545–0.565 μm) and 6 (1.628–1.652 μm) for Terra and bands 4 and 7 (2.105–2.155 μm) for Aqua, which record reflectance in the green and short-wave infrared ranges of the spectrum, respectively. A statistical linear relationship between NDSI and snow fraction in a MODIS pixel was established by using higher resolution Landsat snow maps as an estimate of reference snow cover fraction. This method (Salomonson & Appel, 2004, 2006) is currently used to create the standard MODIS/Terra Snow Cover Daily L3 Global 500 m Grid (MOD10) product (Hall et al., 1995, 2002; Riggs et al., 2006). The only previous validation of this approach was that orginally performed during algorithm development (Salomonson & Appel, 2004, 2006).

Machine learning represents an alternative to the statistical methods for estimating snow fraction. Artificial neural networks (ANNs) are a machine learning technique which can learn relationships between specified input and output variables. Neural networks constitute an information processing model that stores empirical knowledge through a learning process and subsequently makes the stored knowledge available for future use (Haykin, 1999). Various remote sensing applications have utilized ANNs for subpixel estimation of a number of surface types (Foody et al., 1997; Lee & Lathrop, 2006; Shabanov et al., 2005; Tatem et al., 2002). Neural networks are advantageous over other approaches as it is unnecessary to assume linear mixing of signals in a pixel. Endmembers are not required and auxiliary information such as land cover is easily incorporated. Once the neural network is trained it is computationally efficient to produce snow fraction maps on both regional and global scales, even though in this application the ANN is trained over North America.

ANNs have been applied in only a few snow studies. Simpson and McIntire (2001) used a recurrent ANN to differentiate between cloud, land, snow-covered and mixed pixels. The mixed pixels were then used in a spectral linear unmixing method to derive snow fraction. ANNs were also applied for deriving SWE and snow depth (Tedesco et al., 2004), and brightness temperatures clusters related to different snow conditions (Sun et al., 1997) from Special Sensor Microwave Imager (SSM/I) brightness temperatures. Most recently, a neural network approach was implemented for predicting changes in snow cover duration and distribution in the Black Forest mountain range of Germany (Sauter et al., 2010).

This study investigated the applicability of ANNs to successful mapping of snow fraction with a particular interest in improving FSC mapping in forests. To accomplish this aim, a mutlilayer feed-forward ANN was trained with backpropagation and tested on Landsat Enhanced Thematic Mapper Plus (ETM+) scenes within North America representative of the different land covers typical of the snow covered portions of the Northern Hemisphere. This attempt did not consider complex mountainous terrain and training and test scenes were selected over relatively flat terrain. Inputs to the network included MODIS land surface reflectance, NDSI, NDVI, and land cover (Table 1).

The reference snow fraction was determined by applying the MODIS binary snow mapping algorithm from the initial MODIS algorithm (Hall et al., 1995) to higher resolution Landsat ETM+ images. The neural network was then trained on nine Landsat snow maps representative of different land covers characteristic of a number of snow covered areas in the Northern Hemisphere. The developed network and the standard MOD10 snow fraction product were then tested on independent pixels from the training scenes and also on four Landsat scenes which were not used during training of the

Table 1
Artificial neural networks inputs.

Input	Description
MOD09GA Band 1	Reflectance in the red portion of the electromagnetic spectrum (620–670 nm)
MOD09GA Band 2	Reflectance in the near infrared portion of the electromagnetic spectrum(841–876 nm)
MOD09GA Band 3	Reflectance in the blue portion of the electromagnetic spectrum (459–479 nm)
MOD09GA Band 4	Reflectance in the green portion of the electromagnetic spectrum 545–565 nm (Painter et al.)
MOD09GA Band 5	Reflectance in the shortwave infrared portion of the electromagnetic spectrum (1230–1250 nm)
MOD09GA Band 6	Reflectance in the shortwave infrared portion of the electromagnetic spectrum (1628–1652 nm)
MOD09GA Band 7	Reflectance in the shortwave infrared portion of the electromagnetic spectrum (2105–2155 nm)
NDSI	Normalized Difference Snow Index $\frac{(Band4-Band6)}{(Band4+Band6)}$
NDVI	Normalized Difference Vegetation Index $\frac{(Band2-Band1)}{(Band2+Band1)}$
Land cover (IGBP)	Yearly land cover classification in the International Geosphere-Biosphere Programme (IGBP) classification system

ANN (Fig. 1). Finally, the snow fraction maps produced through the ANN approach were compared to the MOD10 snow fraction product.

2. Satellite images and reference snow fraction

2.1. MODIS surface reflectance

MODIS is the primary global environmental monitoring instrument aboard the Terra and Aqua satellites. MODIS acquires images from every location on Earth at least once every 1 or 2 days in 36 discrete spectral bands, cloud-cover permitting (Barnes et al., 1998). Science teams have developed a variety of standard data products which are distributed free of charge. The MODIS Surface Reflectance Daily L2G Global 500 m and 1 km product provides surface spectral reflectance in seven bands in the visible and near-infrared portion of the electromagnetic spectrum and is corrected for atmospheric effects (Vermote et al., 2011). The product is distributed by the Land Processes Distributed Active Archive Center: https://lpdaac.usgs.gov. The seven land surface reflectance bands at 500 m spatial resolution were used in the study. The product also contains ancillary datasets describing cloud cover and data quality for each pixel and these were used to exclude from further analysis pixels that were identified as cloud-covered, mixed, fell within cloud shadow or were less than ideal quality. Water was also excluded from the analysis using a water mask acquired from MODIS land cover product. The datasets in the surface reflectance product are provided in a sinusoidal projection. In the current study they were re-projected to a UTM projection with a WGS84 datum to match the projection of the respective Landsat scenes.

2.2. Landsat reference snow fraction maps

Selection of Landsat ETM+ training and test scenes was restricted to partially snow-covered images acquired within North America during different months of the snow season. The scenes (Table 2) were also selected for minimal cloud cover and were acquired between 2000 when MODIS became operational and 2003 when the Landsat ETM+ Scan Line Corrector (SLC) failed which degraded the ETM+ image quality. The main objective in selecting the training scenes was to represent land covers typical of the snow covered mid- to high-latitudes. Land cover classification in the International Geosphere-Biosphere Programme (IGBP) classification scheme was provided in the Terra Land Cover 96 Day L3 Global 1 km Integerized Sinusoidal (ISIN) Grid (MOD12) product (Friedl et al., 2002). The land cover classification system used in selecting samples collapsed the seventeen IGBP land cover classes into eight: evergreen forest, deciduous forest, mixed forest, mixed agriculture, barren/sparsely vegetated, savannas, grasslands/shrublands and wetlands (Table 3). A similar approach was used previously by Hall et al. (2001) to assess the accuracy of the MODIS snow product. Two of the selected training scenes were previously used in developing the standard MODIS MOD10 snow fraction product (Salomonson & Appel, 2004, 2006). The careful selection of Landsat ETM+ scenes ensured that the neural

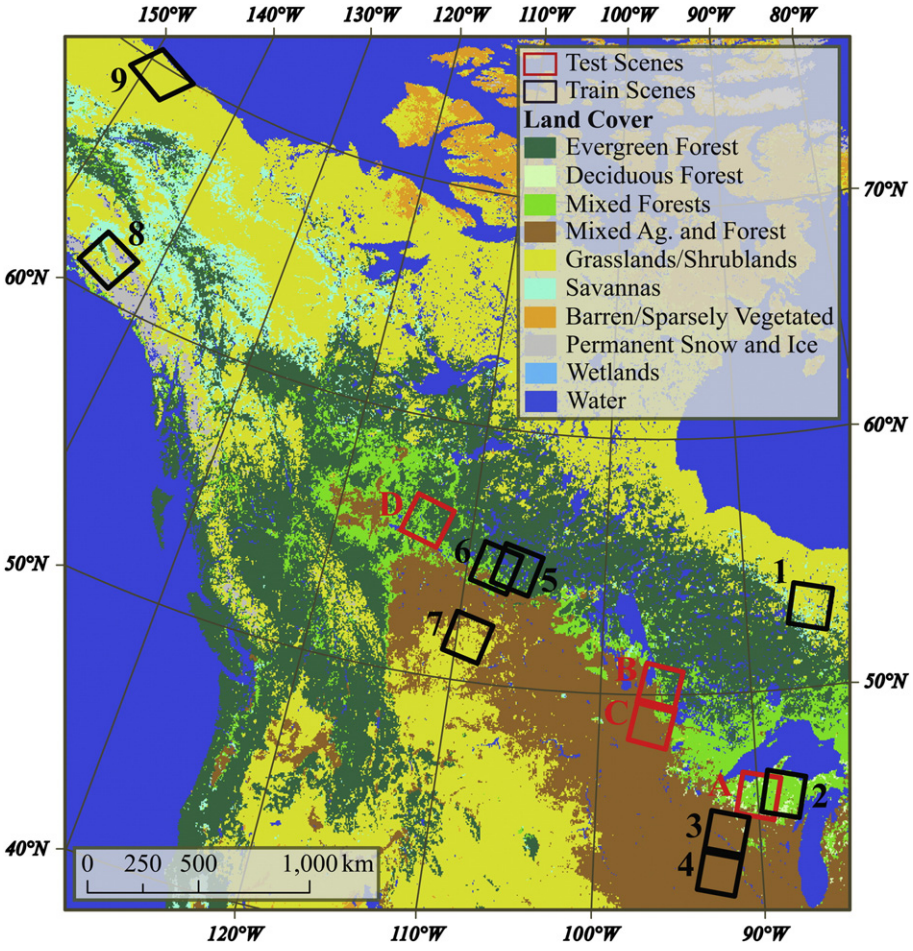

Fig. 1. Training and test Landsat scenes were located in North America. Training sites were selected to be representative of different land covers and snow fractions.

Table 2
Landsat ETM+ training (1 through 9) and test (A, B, C and D) scenes.

Scene	WRS-2 path/row	Date acquired	Land covers	Number of training samples	Number of test samples
Training scenes					
1[a,b]	24/23	04/24/2000	Savannas, grasslands/shrublands, wetlands	4366	88,285
2	24/28	12/10/2002	Deciduous forests, mixed forests, mixed agriculture	5826	58,972
3	26/29	02/07/2002	Deciduous forests, mixed forests, mixed agriculture	2408	93,063
4	26/30	02/07/2002	Mixed agriculture	1281	123,430
5	38/22	03/18/2003	Evergreen forests, mixed forests, savannas	2207	67,871
6	39/22	11/01/2002	Evergreen forests, mixed forests, mixed agriculture, savannas	4506	56,376
7	39/24	11/01/2002	Mixed agriculture, grasslands/shrublands	2,000	72,078
8[a,b,c]	65/17	05/12/2001	Savannas, grasslands/shrublands	3308	73,156
9[a,b,c]	73/11	05/23/2002	Barren/sparsely vegetated, grasslands/shrublands	1772	55,006
Test scenes					
A	25/28	04/08/2003	Deciduous forests, mixed forests, mixed agriculture	0	96,282
B	30/25	05/10/2002	Evergreen forests, mixed forests, mixed agriculture	0	42,527
C	30/26	03/20/2001	Evergreen forests, mixed forests, mixed agriculture	0	116,151
D	43/21	04/19/2002	Evergreen forests, mixed forests	0	116,874

[a] Modified Black Body Atmospheric correction used instead of FLAASH.
[b] Additional georeferencing was not performed.
[c] Scene used in developing MODIS FSC product (Salomonson & Appel, 2004, 2006).

network was trained and tested over areas representative of North American winter conditions.

The Landsat ETM+ images were obtained free of charge from the United States Geological Survey (USGS) Earth Resources Observation and Science (EROS) data center: http://glovis.usgs.gov. This product was provided after correction from distortions related to sensor, satellite and Earth effects. Each of the Landsat ETM+ images was converted to radiance using a standard approach (Chander et al., 2009). Conversion to reflectance and atmospheric correction was then performed using the Fast Line-of-sight Atmospheric Analysis of Spectral Hypercubes (FLAASH) method as implemented in ENVI 4.5 software package (Kaufman et al., 1997). For three of the scenes FLAASH was unsuccessful due to the absence of a dark object in these snow covered scenes and therefore a simpler modified black body correction (Chavez, 1988) was applied. The atmospherically-corrected scenes were compared to orthorectified Landsat ETM+ images which were acquired through the Global Land Cover Facility: http://glcf.umiacs.umd.edu. Most of the scenes were then georegistered through selection of Ground Control Points (GCPs) to compensate for geolocation differences between the orthorectified scenes and those used in the study. In these cases at least fifteen GCPs were selected for each scene with a root mean square error of less than 0.1 pixels. Any portion of the scenes that was cloud-covered or shadowed by clouds was masked and excluded from further analysis.

Table 3
Land cover classes used in the study.

Original IGBP land cover classes	Reclassified land cover classes
Evergreen needleleaf forest	Evergreen forests
Evergreen broadleaf forest	
Deciduous needleleaf forest	Deciduous forests
Deciduous broadleaf forest	
Mixed forests	Mixed forests
Croplands	Mixed agriculture
Urban and built-up	
Cropland/natural vegetation mosaic	
Barren/sparsely vegetated	Barren/sparsely vegetated
Woody savannas	Savannas
Savannas	
Closed shrublands	Grasslands/shrublands
Open shrublands	
Grasslands	
Permanent wetlands	Wetlands
Permanent snow and ice	n/a
Water	n/a

The pre-processed Landsat ETM+ images were then used as input to a snow cover mapping algorithm (Hall et al., 1995) which classified pixels as either snow-covered or snow-free. The classification algorithm is the Landsat ETM+ equivalent of the algorithm used for the production of the standard MODIS binary snow cover product. These 30 m Landsat binary snow maps were used to calculate snow fraction within each MODIS pixel. Snow fraction was calculated as percent snow covered area to the total area within a 750 m radius of the center of a MODIS pixel. The study did not calculate the percent snow cover within the exact area delimited by a MODIS pixel because of reported MODIS geolocation uncertainties (Wolfe, 2006; Wolfe et al., 2002). Calculating the snow fraction within a larger spatial footprint than the pixel extent is a common approach for dealing with the geolocation uncertainties. For example, in the validation of the snow fraction method described by Painter et al. (2009) sampling was performed within a circular footprint with radius ranging from 500 m to 2000 m. In this study, a 750 m radius from the center of each MODIS pixel was applied to delimit the area from which the snow fraction value of the pixel was calculated (Fig. 2).

3. Methodology

3.1. Artificial neural networks (ANNs)

ANNs constitute an information processing model that stores empirical knowledge and subsequently makes the stored knowledge available for future use. ANNs are loosely modeled after the brain of living organisms and resemble the brain in that knowledge is acquired from the environment through a learning process and is stored in the form of interneuron connection strengths (Basheer & Hajmeer, 2000; Haykin, 1999).

The fundamental processing unit of ANNs is the neuron. A neuron consists of connection links (synapses) characterized with certain weights (strength). Input is passed from one end of the synapse, multiplied by the connection weight and passed on to the summing junction (adder) of the neuron. The adder sums the weighted inputs:

$$u_k = \sum_{j=1}^{m} w_{kj} x_j \quad (1)$$

where x_j represents the j^{th} input signal from a total of m inputs; w_{kj} represents the strength of the connection weight from the j^{th} input signal to neuron k, and u_k is the sum of the weighted input signals.

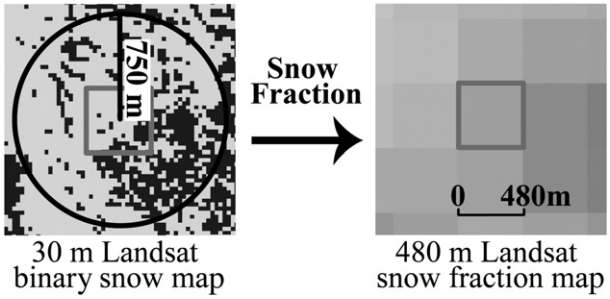

Fig. 2. Binary snow cover maps were resampled to MODIS resolution within a 750-m circular radius around each MODIS pixel.

A bias b_k is added to the linear combined output u_k to derive the activation potential of v_k of the neuron:

$$v_k = u_k + b_k \quad (2)$$

The activation potential v_k is then passed to the transfer (activation or squashing) function φ, which computes the output y_k of the neuron:

$$y_k = \varphi(v_k) \quad (3)$$

The two most common transfer functions are the threshold and sigmoid functions (Haykin, 1999). The threshold function returns discrete output values depending on whether a neuron's activation potential is above or below a predefined threshold. The sigmoid function returns a continuous range of output values and is the most common transfer function (Haykin, 1999). It has a typical S-shape curve which balances linear and nonlinear behavior. Furthermore, it is differentiable, which is necessary for some types of supervised neural network learning methods including backpropagation used in this study.

This study examined the two common sigmoid transfer functions, the logistic sigmoid and tangent hyperbolic functions, and found the ANN performed better with the latter. The tangent hyperbolic function returns an output between −1 and 1:

$$\varphi(v_k) = \tanh(v_k) \quad (4)$$

Neurons are connected to each other through their connection links. Thus, the output of a neuron is transmitted through a connection link, multiplied by the weight of the connection link and passed to the summing junction of the next neuron.

The structure of neurons in an ANN is determined by the network's architecture. Typically, neurons are arranged in layers. The input layer does not consist of neurons, but rather of nodes which pass each input element to the first layer of neurons. In remote sensing, an input layer is the available information about a pixel such as surface reflectance or land cover. Each of the neurons in the first hidden layer receives weighted signal from the input layer and computes an output which is then passed to all of the neurons in the next hidden layer. The neurons in the final hidden layer pass their output to each of the neurons in the output layer. The output of each output layer neuron is returned as the output of the ANN.

In the current application, a multilayer feedforward ANN with one hidden layer is used. The ANN is feedforward, as opposed to recurrent, which means that the network does not include any feedback loops, i.e. inputs to a neuron are not influenced by the output of that neuron. In this multilayer feedforward ANN the input layer of source neurons (surface reflectance, NDSI, NDVI and land cover of a pixel) project to a hidden layer of neurons which projects directly to the output layer, the snow fraction for the pixel.

ANNs learn an environmental model to achieve a specified goal. In this study the model of the environment is the relationship between surface reflectance, vegetation and snow indices, land cover, and snow fraction. The specific goal is deriving snow fraction from remote sensing products. The network acquired the knowledge from observations of the environmental variables through a training process during which labeled inputs were paired with desired responses. During the backpropagation learning phase network weights were randomly initialized and the error was calculated as the difference between the generated and the target outputs. The error was then backpropagated through the network and the weights were adjusted to minimize the error. The process was repeated iteratively until the error reached a predefined minimal value or until the generalization performance of the network deteriorated based on a set of examples excluded from the training. Network generalization refers to how well an ANN performs on input not used in training the network. The set of examples used for assessing the generalization performance during training is called validation set.

3.2. Training dataset

As the performance of ANNs trained in a supervised manner is closely related to the quality of the training dataset (Priddy & Keller, 2005), the dataset must be representative of the areas of interest. In the current study, the training examples were selected to not be biased towards a particular land cover but instead to adequately represent the land covers typical of mid- and high-latitude snow covered environments. The training set was also developed to not be biased towards a particular snow cover fraction. For example, if the training samples were mostly of high snow fraction then the ANN would adjust its weights for calculating high snow fraction well, but may be less accurate over pixels with small snow fraction.

To achieve these objectives a total of nine Landsat snow maps (Fig. 1; Table 2) were sampled to create the training and validation datasets. The samples comprised between 1 and 7% of all available pixels within each Landsat scene. Following usage in the ANN literature both the training and validation datasets were used during network training. The samples from the training dataset were used in adjusting the weights of the ANN. The validation dataset was used during training to measure the generalization performance of the network as represented by the mean square error (MSE) between the network-derived and the Landsat-derived FSC. Training ended when MSE of the validation dataset began to increase indicating that further training would decrease the generalization abilities of the network (Haykin, 1999).

To minimize training bias towards any land cover or snow cover fraction, sample points were selected through stratified random sampling. Stratification was performed per snow cover fraction which was categorized in 0.1 FSC intervals and by land cover category. Within ArcGIS the land cover of each Landsat ETM+ training scene was examined. All pixels from prevalent land cover categories were extracted and assigned to the appropriate FSC category. From these stratified pixels, a random selection was performed. Prevalent land cover categories as well as number of random pixels extracted were determined subjectively in an attempt to create equal representation of land cover and snow fraction categories in the sample dataset with similar number of samples from each training scene. The final dataset included 27,674 observations. These observations while grouped according to land cover and snow fraction categories were randomly split in three subsets. Half of these observations comprised the training dataset and a quarter comprised the validation dataset. The remainder was withheld as an independent test dataset. The complete dataset was fairly representative of the different land cover and snow fraction categories. As can be seen in Fig. 3 evergreen forests, mixed forests and mixed agriculture and forest were best represented, while barren and sparsely vegetated areas were less well represented.

3.3. Training

The multilayer feedforward ANN was trained with backpropagation to compute the fraction of snow in individual MODIS pixels. Ten inputs were provided to the network (Table 1) including the seven MODIS surface reflectance bands, NDSI, NDVI and land cover in the IGBP classification scheme. Calculated NDSI and NDVI were added to emphasize snow-covered and vegetated areas, respectively. NDVI is a normalized difference ratio of bands in the red and near-infrared portions of the electromagnetic spectrum and is one of the vegetation indices used to indicate presence of healthy green vegetation (Jensen, 2005). Land cover in the IGBP classification scheme was also selected as an input because spectral characteristics of snow are known to vary across land covers (Hall et al., 1995; Moody et al., 2007) and the

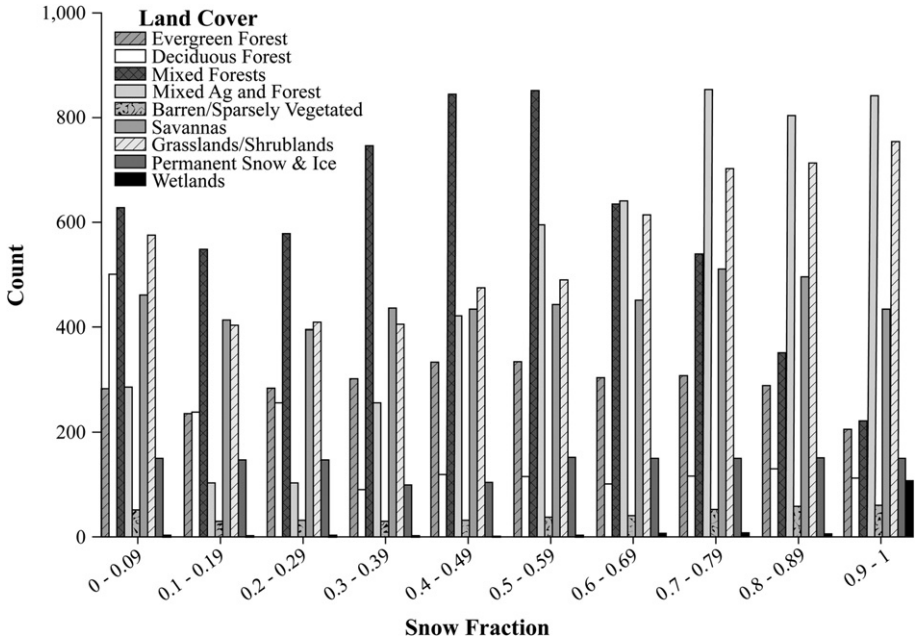

Fig. 3. Sample points used in final ANN.

reflectance of snow-free surfaces depends on the surface type. The complete 17-class IGBP classification system was used as input to the ANN so that network weights reflect differences in land covers.

An alternative land cover input scheme was also tested where each IGBP class was represented in the network as a separate binary input and presence or absence of the class was coded as 1 or 0, respectively. For this approach a total of 25 inputs were passed to the network. The results of both land cover coding methods were similar with the binary land cover coding found to be slightly less accurate. The categorical land cover input was selected for the final network.

In creating the final network the following network properties were determined through a trial-and-error procedure: (1) the number of hidden-layer neurons, (2) the input-to-hidden transfer function and (3) the input-output normalization method. The neural network was trained using several different configurations and the performance of a trained networks were analyzed in terms of RMSE and R^2 as well as by visually comparing resulting ANN FSC maps to the Landsat-derived reference FSC maps. To ensure differences in the snow fraction accuracies were not due to differences in initial weights, initial weights were held constant while determining network properties. The properties of the final network are summarized in Table 4 where MSE refers to the performance measure used by the neural network training algorithm during the validation stage of the training process.

Table 4
Summary of properties of the developed ANN.

ANN Property	Description
Training method	Levenberg–Marquardt backpropagation (supervised)
Learning method	Gradient descent with momentum weight and bias
Performance measure	Mean square error (MSE)
Network architecture	Ten input neurons, one hidden layer with twenty hidden-layer neurons, and one output neuron
Transfer functions	Tangent hyperbolic between input and hidden layers; linear between hidden and output layers
Input/output normalization	Each input band is scaled between −1 and 1

The selected final network used a single hidden layer and the number of hidden-layer neurons was twenty — twice the number of inputs. Experimenting with 10 and 30 hidden-layer neurons and with a greater number of hidden layers did not provide an improvement of the snow fraction accuracies. Therefore this study used the simpler network which has been found in other studies to be able to learn any relationship between input and output (Priddy & Keller, 2005). For the alternative IGBP input scheme, 50 hidden layers were used which was similarly two times the number of inputs, but were found to produce slightly less accurate snow fractions. The final neural network generated fewer than 5% physically unreliable snow fractions (i.e., above 1 or below 0). These fractions were adjusted to the appropriate minimums and maximums.

3.4. Testing

The performance of the ANN snow fraction method was tested in two stages. First, pixels which were withheld from training but extracted from the training scenes were compared to Landsat estimates. This first test dataset included all non-masked pixels from the reference Landsat scenes excluding the pixels extracted through the stratified random sampling. Second, pixels from reference scenes not used for training were compared to Landsat estimates. The second dataset included all non-masked pixels from the independent test scenes. The second option represents a fairly rigorous comparison.

The accuracies of the snow fraction estimates of the ANN with respect to the reference Landsat estimates were compared to the accuracies of both the binary and FSC datasets in the standard MODIS MOD10 snow cover product (Riggs et al., 2006). Testing was also performed on each land cover category separately.

Network performance was measured by calculating the root mean square error (RMSE) between estimates and reference snow fractions:

$$\mathrm{RMSE} = \sqrt{\frac{1}{n-1} * \sum_{i=1}^{n} (x' - x)^2} \quad (5)$$

where n is the number of samples, x′ is the estimated FSC and x is the reference FSC. The correlation of determination (R^2) which is the square of the Pearson correlation coefficient was also used as

Table 5
RMSE and R^2 of ANN and MOD10 FSC and reference FSC of train and test scenes.

	Number of test samples	ANN[a]		ANN[b]		MOD10 FSC		MOD10 binary	
		R^2	RMSE (%)	R^2	RMSE (%)	R^2	RMSE (%)	R^2	RMSE (%)
Train scenes	781809	0.90	0.12	0.89	0.13	0.87	0.14	0.53	0.33
Test scenes	371834	0.87	0.14	0.85	0.20	0.88	0.14	0.75	0.26
Test scene A	96282	0.91	0.14	0.88	0.22	0.90	0.13	0.86	0.17
Test scene B	42527	0.75	0.21	0.82	0.21	0.82	0.19	0.73	0.28
Test scene C	116151	0.81	0.14	0.70	0.20	0.84	0.14	0.65	0.24
Test scene D	116874	0.90	0.13	0.87	0.17	0.90	0.12	0.66	0.32

[a] ANN where land cover was input as 1 categorical variable (1LC).
[b] ANN where land cover was input as 16 binary variables (16LC).

performance indicator. R^2 shows how much of the variance of the reference snow fraction is explained by the estimated snow fraction.

The total extent of snow cover according to the reference and estimated snow fractions was also calculated. This provided an indicator of what the actual differences in snow covered area would be if the lower resolution MODIS-estimated snow fractions were used instead of the Landsat-derived ones. To facilitate the comparison, percentage of snow covered to the total area and then difference between the percentages of the estimates and reference snow maps were calculated.

The trained ANN is computationally efficient. For example, on a 3 GHz Intel Core2 Duo CPU the trained ANN required only 7 second of CPU time to run the MATALB script for an image of 116,151 pixels. Of this time, only 0.6 second of CPU time was necessary for normalizing the input, running the ANN, and reverse-normalizing the snow fraction output. The remainder was spent on reading the input, loading the ANN and writing the snow fractions to a file.

4. Results

The developed neural network was able to successfully map snow fraction using MODIS surface reflectance, NDSI, NDVI and land cover as inputs. The mapping accuracy of the test pixels from the training scenes was good with an average R^2 of 0.9 and RMSE of 0.12 (Table 5). The ANN performed slightly less well on four independent test scenes with an average R^2 of 0.87 and RMSE of 0.14. Similar accuracies were found for the MOD10 snow fraction product with an average R^2 of 0.87 and 0.88 over the training and test scene, respectively and with RMSE of 0.14 for both datasets. The binary snow cover MOD10 product compared less well to the Landsat fractional snow cover maps with R^2 of 0.33 and 0.26 and RMSE of 0.53 and 0.75 for training and test scenes, respectively. ANN estimates of total snow covered area were only 2% and 3% less than the reference snow cover extent for the training and test scenes, respectively (Table 6). The MOD10 fractional snow product differed from the reference areas by 4% more and 2% less than the reference for the training and test scenes, respectively. There were much larger differences in total snow covered area for the binary MOD10 product.

Maps of ANN-estimated snow fractions illustrated that the neural network was able to recreate the snow cover spatial distribution. For test scene A illustrated in Fig. 4, ANN snow fractions have a high R^2 of 0.91 compared to the reference; however, they do not fully capture the snow cover variability in the reference snow map. The ANN also tended to underestimate snow cover at high snow fractions. The MOD10 snow fraction map of this test scene better preserved the snow cover variability but the actual snow cover was still underestimated. Conversely, for test scene C, also shown in Fig. 4, both the ANN and MOD10 performed slightly worse with respect to percentage variance explained (R^2 of 0.81 and 0.82, respectively) but captured the spatial variability in snow fraction over the scene. However, the ANN snow map was more similar to the reference snow map than that of MOD10. Both ANN and MOD10 overestimated the snow cover in test scene C at 4% and 6%, respectively (Fig. 6; Table 6).

4.1. Mapping accuracy by land cover

An objective of the study was to examine if estimating snow fraction in forested areas could be improved through a nonlinear mapping technique such as ANN. To analyze this outcome, mapping accuracy by land cover was analyzed for both the training and independent test scenes. Accuracy assessment was undertaken for both the ANN snow fraction maps produced in this study and the standard MOD10 snow fraction product to facilitate inter-comparisons.

4.1.1. Training scenes dataset

No distinct difference in the snow fraction accuracy between forested and non-forested areas was found for the ANN fractional snow cover maps. For the training scenes, non-forested classes have slightly greater accuracy (R^2 ranging between 0.92 and 0.94 and RMSE ranging between 0.11 and 0.13) than evergreen and mixed forest classes. Deciduous forests had mapping accuracy on par with non-forested areas as demonstrated by R^2 of 0.94 and a low RMSE of 0.09. In contrast, snow fraction was much more poorly mapped in evergreen forests (R^2 of 0.82 and RMSE of 0.15). Mixed agriculture and forest which had the largest number of comparison samples also had the lowest accuracies with an R^2 of 0.74 and RMSE of 0.11. MOD10 mapping accuracies, while slightly lower than ANN (Table 7), exhibited similar patterns across the different land covers. For example, R^2 for deciduous forests was 0.90 and RMSE was 0.11 while R^2 for evergreen forests was 0.77 and RMSE was 0.19.

Table 6
Snow cover extent in square kilometers and as percentage of total area of the three test scenes individually and combined.

	Total area	Reference	ANN[a]	ANN[b]	MOD10 FSC	MOD10 binary
Train scenes	172059/100	107855/63	104692/61	102767/60	114763/67	137875/80
Test scenes	92959/100	54058/58	50762/55	43682/47	51978/56	63906/69
Test scene A	24071/100	17372/72	15313/64	13228/55	16053/67	19614/81
Test scene B	10632/100	5091/48	4032/38	3698/35	3906/37	5957/56
Test scene C	29038/100	21588/74	22555/78	18734/65	23159/80	24745/85
Test scene D	29219/100	10006/34	8862/30	8023/27	8860/30	13591/47

[a] ANN where land cover was input as 1 categorical variable (1LC).
[b] ANN where land cover was input as 16 binary variables (16LC).

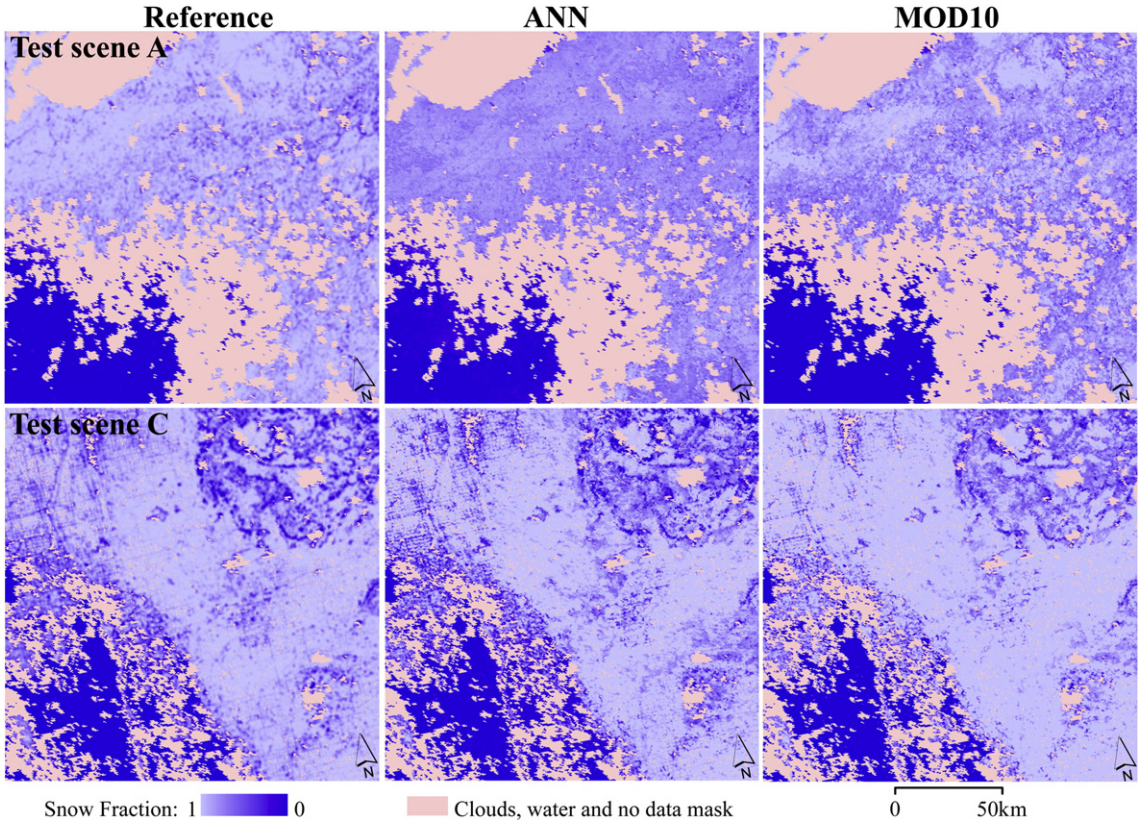

Fig. 4. Snow maps over (a) test scene A and (b) test scene C. Snow maps show pixels covered with large snow fraction as light blue and snow-free pixels as dark blue.

There do not appear to be significant differences between land covers in terms of the absolute areal extent of mapped snow cover (in km^2) as illustrated in Fig. 5 and Table 8. ANNs performed the best over savanna with less than a 1% difference in area from the reference. Outside of savanna, total snow covered area was best mapped by the ANN for the three forested land covers. Total snow cover extent was overestimated by only 1% over deciduous forests and by 5% over evergreen forests which suggests that ANNs are performing well in forests. Compared to the ANN, MOD10 provided more accurate total snow cover extents for the non-forest classes but was less accurate over forests than the ANN overestimating the snow cover by 3% for deciduous and by 9% for evergreen forests (Table 8).

4.1.2. Test scenes dataset

The four test scenes provided a more rigorous validation of the ANN FSC maps as these scenes were not used in its training. Not surprisingly, accuracy as measured by R^2 and RMSE were somewhat lower for the test than training scenes with the surprising exception of mixed agriculture (Fig. 6; Table 7). MOD10 displayed higher accuracy for all land covers.

Table 7
RMSE and R^2 of ANN and MOD10 FSC and reference FSC for different land covers.

	Number of test samples	ANN[a]		ANN[b]		MOD10 FSC		MOD10 binary	
		R^2	RMSE (%)	R^2	RMSE (%)	R^2	RMSE (%)	R^2	RMSE (%)
Train scenes									
Evergreen forests	117940	0.82	0.15	0.79	0.16	0.77	0.19	0.29	0.52
Deciduous forests	20042	0.94	0.09	0.92	0.10	0.90	0.11	0.61	0.36
Mixed forests	69475	0.87	0.12	0.80	0.15	0.82	0.14	0.46	0.47
Mixed agriculture & forest	257610	0.74	0.11	0.73	0.12	0.68	0.12	0.37	0.21
Barren/Sparsely vegetated	2123	0.92	0.13	0.91	0.14	0.90	0.15	0.86	0.18
Savannas (Tundra)	44161	0.92	0.12	0.91	0.12	0.87	0.15	0.52	0.39
Grasslands/shrublands	158310	0.94	0.11	0.93	0.12	0.90	0.13	0.78	0.23
Test scenes									
Evergreen Forests	90127	0.81	0.16	0.86	0.15	0.83	0.15	0.65	0.35
Deciduous Forests	22016	0.95	0.13	0.97	0.12	0.95	0.12	0.97	0.09
Mixed forests	132240	0.88	0.14	0.90	0.23	0.88	0.14	0.75	0.25
Mixed agriculture & forest	117870	0.86	0.13	0.79	0.20	0.90	0.13	0.81	0.20
Savannas (Tundra)	5357	0.86	0.16	0.86	0.16	0.91	0.14	0.78	0.23
Grasslands/shrublands	3908	0.87	0.15	0.90	0.16	0.92	0.13	0.66	0.29

[a] ANN where land cover was input as 1 categorical variable (1LC).
[b] ANN where land cover was input as 16 binary variables (16LC).

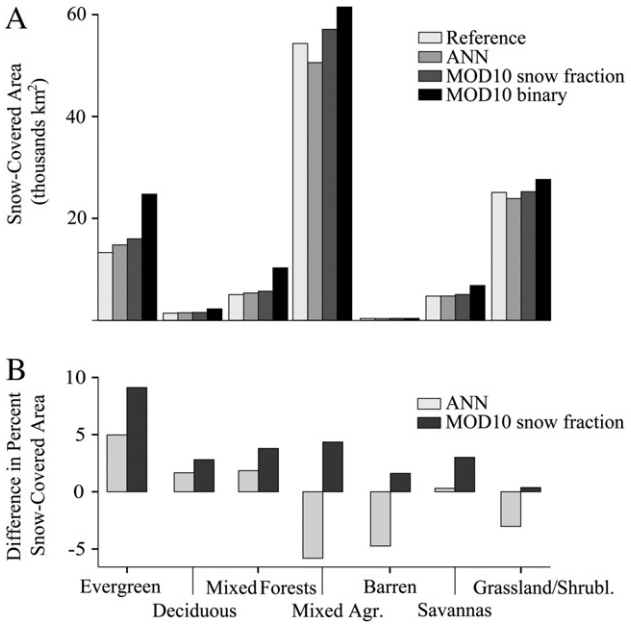

Fig. 5. Snow covered area for test pixels over the training scenes was calculated; (a) total snow cover extent and (b) difference in percentages of snow cover extent for the different land covers.

Both ANN and MOD10 accuracies of estimated snow cover extent (Fig. 6; Table 6) are better for the non-forested category and the mixed agriculture and forest category than over the forest land cover category. ANN estimated the snow cover extents more accurately than MOD10 over deciduous forests and mixed agriculture and forests, while MOD10 provided better estimates over the other land covers. The differences between ANN and MOD10 over evergreen and mixed forests were very small — 1% and 2%, respectively.

To further investigate differences in mapping accuracy over land covers, scatter plots of estimated versus reference snow fractions were created (Fig. 7). Both ANN and MOD10 show large scatter indicating a large range of errors in the snow fraction estimates at the individual pixel level. ANN scatter plots also indicated a tendency to underestimate snow-covered area at higher snow fractions. The MOD10 scatter plots show a large number of snow fractions erroneously estimated as 100% or 0%. Similar to the other accuracy indicators, the scatter plots do not show marked differences across land cover categories.

4.2. Comparison to linear spectral unmixing

The overall mapping accuracy of the ANN snow fraction maps compares well with accuracies of published linear spectral unmixing snow fraction approaches. SnowFrac which was developed and tested over Norway and Switzerland has a reported R^2 of 0.95 and 0.85 (Vikhamar & Solberg, 2002) which is a similar R^2 to the ANN FSC. The most recent study of linear mixture analysis for FSC mapping (Painter et al., 2009), reported an average RMS error of 5% for validation scenes located in the Colorado Rocky Mountains, the Sierra Nevada of California, the headwaters of the Rio Grande, and the Himalayas. Due to topography, barren areas, brush, meadows and alpine savannas were present at high altitudes while coniferous and deciduous forests were present at the lower elevations of the validation areas.

However, these studies did not report error analysis by land cover. In addition, ANN has two advantages over these approaches. The first is that there is no need to assume linear mixing of the surfaces present in a pixel. Such an assumption may by problematic over forested areas due to presence of tree canopy yet as demonstrated in the results the ANN approach performed similarly in forested and non-forested areas. The second advantage of an ANN over linear unmixing is that it is computationally very efficient because once the network is trained it only needs to reference the saved connection weights and snow fraction is calculated through multiplication and summation. Unlike linear unmixing there is no need to refer to spectral libraries or solve for the snow fraction of every pixel. It is possible to expand the training of the ANN for better global applicability by adding additional training scenes from other snow covered regions (e.g., scenes from Asia, Europe and South America) or a broader range of snow cover conditions. The improved ANN will still have the same number of connection weights and the same computational cost as the ANN presented in this study. The linear unmixing approach presented by Painter et al. (2009) reported a 90 minute CPU time required to produce the snow map for a test scene in its research mode. The computational requirements of the method in its operation mode were reported to be similar to the ANN computational requirements.

5. Discussion

No distinct differences in snow mapping accuracies were found across land covers or between the ANN developed in this study and the current standard MOD10 snow cover fraction product. The lack of major differences in ANN accuracy between training and test dataset indicated the good generalization ability of ANN over areas that it was

Table 8
Snow cover extent in square kilometers and as percentage of total area of land covers from train and test scenes.

	Total area	Reference	ANN[a]	ANN[b]	MOD10 FSC	MOD10 binary
Train scenes						
Evergreen forests	29485/100	13308/45	14773/50	13489/46	15993/54	24784/84
Deciduous forests	5011/100	1384/28	1468/29	1488/30	1525/30	2235/45
Mixed forests	17369/100	5048/29	5369/31	4892/28	5706/33	10290/59
Mixed agriculture & forest	64403/100	54321/84	50580/79	50248/78	57124/89	61484/95
Barren/sparsely vegetated	531/100	364/68	338/64	333/63	372/70	377/71
Savannas (Tundra)	11040/100	4736/43	4770/43	4838/44	5069/46	6826/62
Grasslands/shrublands	39577/100	25089/63	23888/60	23901/60	25235/64	27648/70
Test scenes						
Evergreen forests	22532/100	8030/36	6919/31	7105/32	7012/31	11769/52
Deciduous forests	5504/100	3891/71	3478/63	3430/62	3455/63	4149/75
Mixed forests	33060/100	19997/60	17928/54	14136/43	18238/55	23971/73
Mixed agriculture & forest	29467/100	20752/70	21131/72	17748/60	21895/74	22638/77
Savannas (Tundra)	1339/100	689/51	632/47	646/48	661/49	722/54
Grasslands/shrublands	977/100	632/65	608/62	558/57	649/66	595/61

[a] ANN where land cover was input as 1 categorical variable (1LC).
[b] ANN where land cover was input as 16 binary variables (16LC).

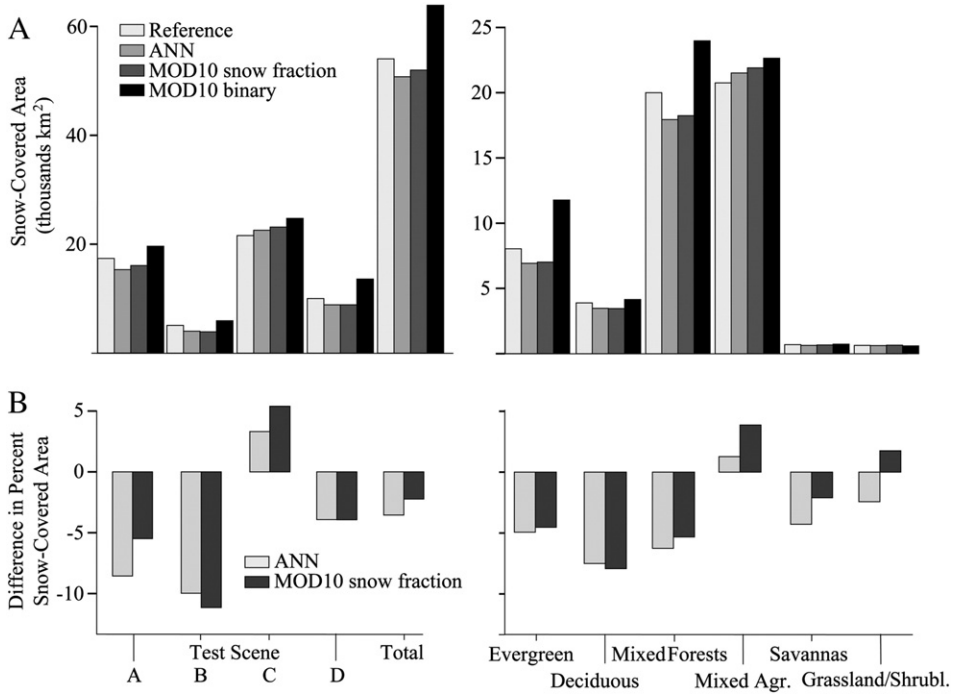

Fig. 6. Snow covered area for the three test scenes and combined, and for the different land covers was calculated; (a) total snow cover extent and (b) difference in percentages of snow covered extent.

not trained on. The MOD10 product also showed consistent performance across land covers. The ANN also compared well to the standard MODIS snow fraction method with a slight advantage in forested areas when tested on the training scenes dataset.

The slight differences in accuracy of ANN across land covers may be attributed to how well each class was represented in the training dataset. However, no relationship between the representativeness of a class in the training dataset and mapping accuracy was found. For example, the barren and sparsely vegetated class was the least represented land cover in the training dataset, and it indeed was one of the land covers with large difference between estimated and reference snow cover extent (Fig. 5). However, the total area of barren and sparsely vegetated areas of the training scenes test dataset was small (531 km^2 compared to 5011 km^2 for deciduous and 29,485 km^2 for evergreen forests). Large differences in the percentage of snow cover extent resulted from only small difference in the actual snow covered area. Furthermore, this land cover exhibited high accuracy as measured by R^2 and RMSE.

ANN performed very well over deciduous forests. This was another land cover that was underrepresented in the training dataset, but ANN performance was not affected. Snow fraction mapping in forests is complicated due to the presence of tree canopy which interferes with the remote sensing signal and is an obstacle to detecting the snow beneath. The better performance of ANN over deciduous forests may be explained by the deciduous trees losing their leaves during the winter.

Mixed agriculture and forests were the most difficult land cover to estimate snow fraction in the training scenes but not the test scenes. This may be related to the large variability of surfaces grouped into this land cover category. For example a wide range of crop type and state, and variable amounts of canopy cover could exist in this category. It was also by far the best represented land cover class in the training dataset.

The developed ANN was trained over test scenes from North America that are representative of the major land covers present in the snow covered portions of the Northern Hemisphere. Mountainous areas were not considered. To potentially achieve better global applicability the ANN could be trained with additional scenes representative of land covers typical of the snow covered areas of Asia, Europe and South America. Training with additional scenes is straightforward and can be quickly implemented using the same approaches developed in this study. Achieving reliable results in high relief areas may be more difficult as shadowing effects would have to be considered. A potential approach could be training the ANN over a range of solar zenith angles and shadow conditions and also expanding the inputs of the network to include slope, aspect and solar zenith angle. Additionally, reference snow maps should be examined to ensure that snow covered areas in shadow are not misclassified as snow-free. As long as the ANN is trained over the areas of interest, it is ready to be used operationally because of its low computational cost.

This study also demonstrated the difference between using the binary MOD10 snow cover maps and the snow fraction MOD10 and ANN maps. In particular, snow cover was considerably overestimated when using the binary snow maps (Figs. 5 and 6; Tables 6 and 8) making fractional snow cover maps a better option for some studies.

This study demonstrated the applicability of neural networks to snow fraction mapping. The developed ANN can be used instead of the standard MODIS snow fraction product because the two methods performed similarly across the test areas. The extensive comparison of the two methods also provided a validation of the standard MODIS snow fraction maps. The standard method exhibited good accuracy with high R^2 and low RMSE.

6. Conclusions

This was the first study that the authors are aware of where an artificial neural network was trained to estimate snow cover fraction. The ANN trained with backpropagation successfully learned the relationship between MODIS snow fraction and surface reflectance in seven wavelength bands, NDSI, NDVI and land cover. The network was applied to both training and independent test scenes and results were compared to reference Landsat snow maps and to the MODIS FSC product. The best performance was achieved over the training

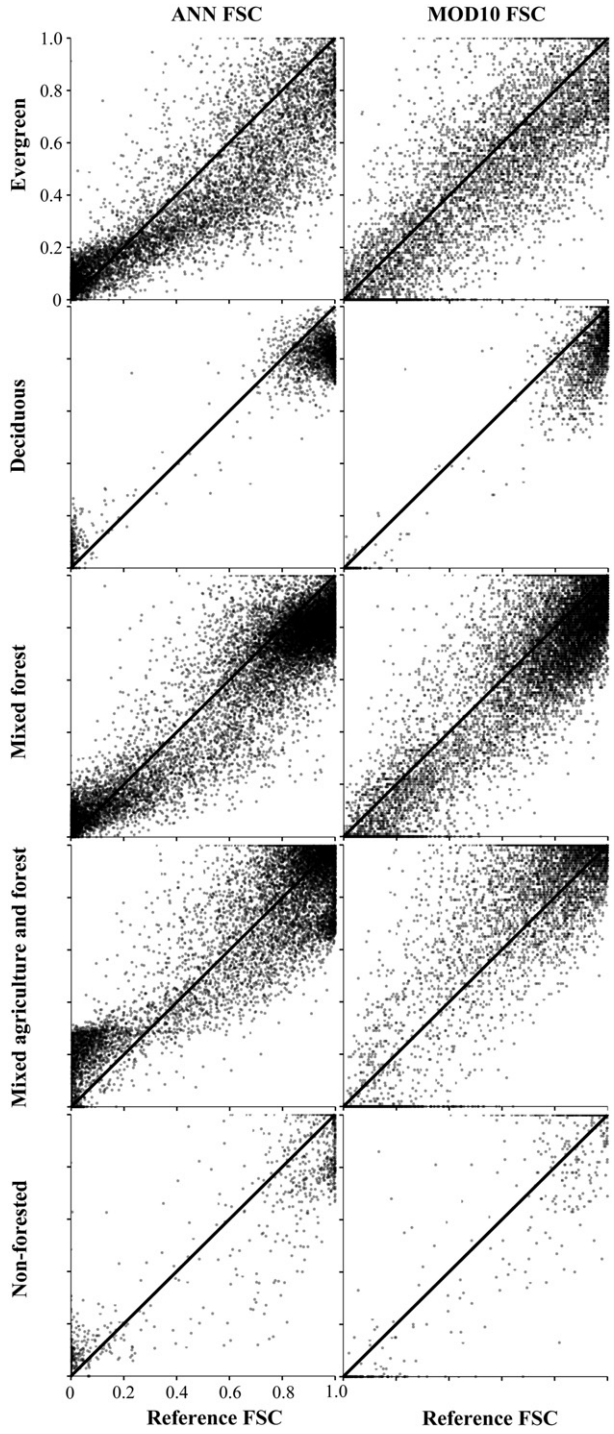

Fig. 7. Scatter plots of test scenes snow fractions for different land cover categories. Scatter plots show ANN and MODIS FSC estimates with respect to the reference FSC. The scatter plots show every 10th pixel in the test scenes dataset.

areas and the performance only slightly decreased when the network had to generalize to independent test areas. There was little difference in ANN performance across the training and test scenes and across different land cover types and it was comparable to the standard MODIS snow fraction product.

An advantage of neural networks over statistical methods such as linear unmixing or regression is that the network makes no assumptions about relationships between the signals of surfaces within pixels or between inputs and outputs. Therefore it was expected that ANN will offer an improvement of snow fraction mapping over forested areas. However, no evidence for that was found when comparing ANN and the standard MODIS snow fraction product. Another advantage of ANN is that once the network is trained it is computationally efficient and it quickly calculates snow fractions. Furthermore, the developed network is easily customizable for specific areas by retraining with additional examples. This study demonstrated that ANNs appear a viable alternative to the existing snow fraction methods.

References

Arnfield, A. J. (2006). Micro- and mesoclimatology. *Progress in Physical Geography*, *30*, 677–689.

Bales, R. C., Molotch, N. P., Painter, T. H., Dettinger, M. D., Rice, R., & Dozier, J. (2006). Mountain hydrology of the western United States. *Water Resources Research*, *42*.

Barnes, W. L., Pagano, T. S., & Salomonson, V. V. (1998). Prelaunch characteristics of the Moderate Resolution Imaging Spectroradiometer (MODIS) on EOS-AM1. *IEEE Transactions on Geoscience and Remote Sensing*, *36*, 1088–1100.

Barnett, T. P., Adam, J. C., & Lettenmaier, D. P. (2005). Potential impacts of a warming climate on water availability in snow-dominated regions. *Nature*, *438*, 303–309.

Basheer, I. A., & Hajmeer, M. (2000). Artificial neural networks: fundamentals, computing, design, and application. *Journal of Microbiological Methods*, *43*, 3–31.

Berry, M. O. (1981). Snow and climate. In D. M. Gray, & D. H. Male (Eds.), *Handbook of snow: Principles, processes, management & use* (pp. 32–59). Toronto: Pergamon Press.

Chander, G., Markham, B. L., & Helder, D. L. (2009). Summary of current radiometric calibration coefficients for Landsat MSS, TM, ETM+, and EO-1 ALI sensors. *Remote Sensing of Environment*, *113*, 893–903.

Chavez, P. S. (1988). An improved dark-object subtraction technique for atmospheric scattering correction of multispectral data. *Remote Sensing of Environment*, *24*, 459–479.

Derksen, C., & LeDrew, E. (2000). Variability and change in terrestrial snow cover: Data acquisition and links to the atmosphere. *Progress in Physical Geography*, *24*, 469–498.

Dickinson, R. E., Oleson, K. W., Bonan, G., Hoffman, F., Thornton, P., Vertenstein, M., Yang, Z. L., & Zeng, X. B. (2006). The community land model and its climate statistics as a component of the community climate system model. *Journal of Climate*, *19*, 2302–2324.

Douville, H., Chauvin, F., Planton, S., Royer, J. F., Salas-Melia, D., & Tyteca, S. (2002). Sensitivity of the hydrological cycle to increasing amounts of greenhouse gases and aerosols. *Climate Dynamics*, *20*, 45–68.

Dozier, J. (1992). Opportunities to improve hydrologic data. *Reviews of Geophysics*, *30*, 315–331.

Foody, G. M., Lucas, R. M., Curran, P. J., & Honzak, M. (1997). Non-linear mixture modelling without end-members using an artificial neural network. *International Journal of Remote Sensing*, *18*, 937–953.

Foppa, N., Wunderle, S., Hauser, A., Oesch, D., & Kuchen, F. (2004). Operational subpixel snow mapping over the Alps with NOAA AVHRR data. *Annals of Glaciology*, 245–252.

Friedl, M. A., McIver, D. K., Hodges, J. C. F., Zhang, X. Y., Muchoney, D., Strahler, A. H., Woodcock, C. E., Gopal, S., Schneider, A., Cooper, A., Baccini, A., Gao, F., & Schaaf, C. (2002). Global land cover mapping from MODIS: Algorithms and early results. *Remote Sensing of Environment*, *83*, 287–302.

Hall, D. K., Foster, J. L., Salomonson, V. V., Klein, A. G., & Chien, J. Y. L. (2001). Development of a technique to assess snow cover mapping errors from space. *IEEE Transactions on Geoscience and Remote Sensing*, *39*, 432–438.

Hall, D. K., Riggs, G. A., & Salomonson, V. V. (1995). Development of methods for mapping global snow cover using moderate resolution imaging spectroradiometer data. *Remote Sensing of Environment*, *54*, 127–140.

Hall, D. K., Riggs, G. A., Salomonson, V. V., DiGirolamo, N. E., & Bayr, K. J. (2002). MODIS snow cover products. *Remote Sensing of Environment*, *83*, 181–194.

Haykin, S. (1999). *Neural networks: A comprehensive foundation* (2nd ed.). Upper Saddle River, NJ: Prentice Hall.

Hongen, Z., & Suhong, L. (2004). Moderate fraction snow mapping in Tibetan Plateau. *International Geoscience and Remote Sensing Symposium* (pp. 3700–3701). Anchorage, AK: IEEE.

Jensen, J. R. (2005). *Introductory digital image processing: A remote sensing perspective* (3rd ed.). Upper Saddle River, NJ: Pearson Prentice Hall.

Kaufman, Y. J., Wald, A. E., Remer, L. A., Gao, B. -C., Li, R. -R., & Flynn, L. (1997). The MODIS 2.1-mm channel-correlation with visible reflectance for use in remote sensing of aerosol. *IEEE Transactions on Geoscience and Remote Sensing*, *35*, 1286–1298.

Klein, A. G., Hall, D. K., & Riggs, G. A. (1998). Improving snow cover mapping in forests through the use of a canopy reflectance model. *Hydrological Processes*, *12*, 1723–1744.

König, M., Winther, J. -G., & Isaksson, E. (2001). Measuring snow and glacier ice properties from satellite. *Reviews of Geophysics*, *39*, 1–27.

Lee, S., & Lathrop, R. G. (2006). Subpixel analysis of Landsat ETM+ using Self-Organizing Map (SOM) neural networks for urban land cover characterization. *IEEE Transactions on Geoscience and Remote Sensing*, *44*, 1642–1654.

Liston, G. E. (1999). Interrelationships among snow distribution, snowmelt, and snow cover depletion: Implications for atmospheric, hydrologic, and ecologic modeling. *Journal of Applied Meteorology*, *38*, 1474–1487.

Marshall, S., Roads, J. O., & Glatzmaier, G. (1994). Snow hydrology in a general-circulation model. *Journal of Climate*, *7*, 1251–1269.
Metsamaki, S. J., Anttila, S. T., Markus, H. J., & Vepsalainen, J. M. (2005). A feasible method for fractional snow cover mapping in boreal zone based on a reflectance model. *Remote Sensing of Environment*, *95*, 77–95.
Moody, E. G., King, M. D., Schaaf, C. B., Hall, D. K., & Platnick, S. (2007). Northern hemisphere five-year average (2000–2004) spectral albedos of surfaces in the presence of snow: Statistics computed from Terra MODIS land products. *Remote Sensing of Environment*, *111*, 337–345.
Niu, G. Y., & Yang, Z. L. (2007). An observation-based formulation of snow cover fraction and its evaluation over large North American river basins. *Journal of Geophysical Research-Atmospheres*, *112*.
Nolin, A. W., & Dozier, J. (1993). Estimating snow grain-size using AVIRIS data. *Remote Sensing of Environment*, *44*, 231–238.
Painter, T. H., Dozier, J., Roberts, D. A., Davis, R. E., & Green, R. O. (2003). Retrieval of subpixel snow covered area and grain size from imaging spectrometer data. *Remote Sensing of Environment*, *85*, 64–77.
Painter, T. H., Rittger, K., McKenzie, C., Slaughter, P., Davis, R. E., & Dozier, J. (2009). Retrieval of subpixel snow covered area, grain size, and albedo from MODIS. *Remote Sensing of Environment*, *113*, 868–879.
Priddy, K. L., & Keller, P. E. (2005). *Artificial neural networks: An introduction.* Bellingham, WA: SPIE Publications.
Rango, A. (1996). Spaceborne remote sensing for snow hydrology application. *Hydrological Sciences*, *41*, 477–494.
Riggs, G. A., Hall, D. K., & Salomonson, V. V. (2006). MODIS snow products user guide to collection 5. http://nsidc.org/data/docs/daac/modis_v5/dorothy_snow_doc.pdf
Roesch, A., Wild, M., Gilgen, H., & Ohmura, A. (2001). A new snow cover fraction parametrization for the ECHAM4 GCM. *Climate Dynamics*, *17*, 933–946.
Romanov, P., Tarpley, D., Gutman, G., & Carroll, T. (2003). Mapping and monitoring of the snow cover fraction over North America. *Journal of Geophysical Research-Atmospheres*, *108*.
Salomonson, V. V., & Appel, I. (2004). Estimating fractional snow cover from MODIS using the normalized difference snow index. *Remote Sensing of Environment*, *89*, 351–360.
Salomonson, V. V., & Appel, I. (2006). Development of the Aqua MODIS NDSI fractional snow cover algorithm and validation results. *IEEE Transactions on Geoscience and Remote Sensing*, *44*, 1747–1756.
Sauter, T., Weitzenkamp, B., & Schneider, C. (2010). Spatio-temporal prediction of snow cover in the Black Forest mountain range using remote sensing and a recurrent neural network. *International Journal of Climatology*, *30*, 2330–2341.
Schowengerdt, R. A. (1997). *Remote sensing: Models and methods for image processing* (2nd ed.). San Diego, CA: Academic Press.
Shabanov, N. V., Lo, K., Gopal, S., & Myneni, R. B. (2005). Subpixel burn detection in moderate resolution imaging spectroradiometer 500-m data with ARTMAP neural networks. *Journal of Geophysical Research-Atmospheres*, *110*.
Shi, J. (1999). Estimating snow fraction using AVIRIS simulated ASTER image in alpine regions. *International Geoscience and Remote Sensing Symposium* (pp. 1795–1797). Hamburg, Germany: IEEE.
Simpson, J. J., & McIntire, T. J. (2001). A recurrent neural network classifier for improved retrievals of areal extent of snow cover. *IEEE Transactions on Geoscience and Remote Sensing*, *39*, 2135–2147.
Simpson, J. J., Stitt, J. R., & Sienko, M. (1998). Improved estimates of the areal extent of snow cover from AVHRR data. *Journal of Hydrology*, *204*, 1–23.
Sun, C. Y., Neale, C. M. U., McDonnell, J. J., & Cheng, H. D. (1997). Monitoring land-surface snow conditions from SSM/I data using an artificial neural network classifier. *IEEE Transactions on Geoscience and Remote Sensing*, *35*, 801–809.
Tatem, A. J., Lewis, H. G., Atkinson, P. M., & Nixon, M. S. (2002). Super-resolution land cover pattern prediction using a Hopfield neural network. *Remote Sensing of Environment*, *79*, 1–14.
Tedesco, M., Pulliainen, J., Takala, M., Hallikainen, M., & Pampaloni, P. (2004). Artificial neural network-based techniques for the retrieval of SWE and snow depth from SSM/I data. *Remote Sensing of Environment*, *90*, 76–85.
Vermote, E. F., Kotchenova, S. Y., & Ray, J. P. (2011). MODIS surface reflectance user's guide, version 1.3. http://modis-sr.ltdri.org/products/MOD09_UserGuide_v1_3.pdf
Vikhamar, D., & Solberg, R. (2002). Subpixel mapping of snow cover in forests by optical remote sensing. *Remote Sensing of Environment*, *84*, 69–82.
Vikhamar, D., & Solberg, R. (2003). Snow cover mapping in forests by constrained linear spectral unmixing of MODIS data. *Remote Sensing of Environment*, *88*, 309–323.
Wolfe, R. E. (2006). MODIS geolocation. *Earth Science Satellite Remote Sensing*Berlin, New York: Springer.
Wolfe, R. E., Nishihama, M., Fleig, A. J., Kuyper, J. A., Roy, D. P., Storey, J. C., & Patt, F. S. (2002). Achieving sub-pixel geolocation accuracy in support of MODIS land science. *Remote Sensing of Environment*, *83*, 31–49.